Enhancing glucose oxidation: exploring 3D Pt nanowire frameworks for electrochemical studies

Tamseel Zaman[1] · Samina Akbar[2] · Joshua S. White[2] · Iris Nandhakumar[2]

Abstract

Here, we report the use of highly reproducible free-standing 3D Pt nanowire frameworks (3D Pt NFs) to investigate the electrochemical oxidation of glucose. To create this unique Pt NFs, we utilize a lipidic bicontinuous cubic phase as a template. The resulting Pt NFs exhibits a unique 3D single diamond morphology with Fd3m symmetry. This intricate structure provides a large surface area and high electrocatalytic efficiency, making it more sensitive to glucose detection. Small Angle X-ray Scattering and Transmission electron microscopy investigations provided valuable insights into the nanoarchitecture of 3D Pt NFs. It highlights the interconnected nature of the nanowires and showcases the potential for optimized electrochemical performance. Very high current densities are registered for the glucose oxidation reactions at 3D Pt NFs during cyclic voltammetry investigations. This knowledge aids in the design and development of advanced electrocatalytic systems, fuel cells, biosensors, and other devices that leverage the unique characteristics of the 3D Pt framework.

Graphical abstract

This study explores 3D Pt NFs for electrochemical glucose oxidation. Using a phytantriol template with two non-intersecting aqueous channels (A), Pt is electrodeposited in one channel (B), resulting in the formation of 3D Pt NFs after template washing (C). This approach demonstrates the potential for efficient glucose oxidation in the structured nanowire frameworks.
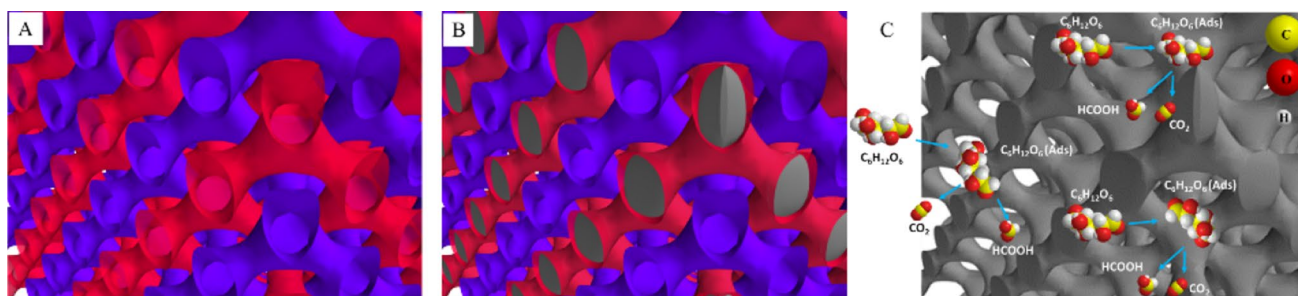
Keywords 3D nanowire framework · Electrooxidation · Glucose · Platinum · Cyclic voltammetry

1 Introduction

The electrochemical oxidation of glucose holds significant importance across diverse fields due to its versatile applications, such as in the development of implantable glucose-powered biofuel cells [1]. Moreover, it contributes to renewable energy systems by converting glucose into electrical energy through fuel cells, offering potential solutions in portable power sources [2]. The electrooxidation of glucose is a fascinating process that involves the oxidation of glucose

✉ Samina Akbar
S.Akbar@soton.ac.uk

1 Department of Natural Sciences and Humanities, University of Engineering and Technology, Lahore (New-Campus), Lahore 54890, Pakistan

2 School of Chemistry, High Field Campus, University of Southampton, Southampton SO17 1BJ, UK

molecules at an electrode surface, typically composed of a noble metal like platinum (Pt) [3]. This electrochemical reaction holds great significance in various fields, including energy conversion, [4] biosensors, [5, 6] and biomedical applications [7]. The electrooxidation of glucose has been studied extensively on bulk Pt and Au, because of their high electrochemical activity [3, 8, 9]. At Pt electrodes, studies have been carried out in acidic [10], basic [11, 12] and neutral media [13].One of the primary challenges in the electrooxidation of glucose is the sluggish reaction kinetics, meaning that the oxidation reaction proceeds at a relatively slow rate. This is primarily due to the strong adsorption of intermediate species formed during the reaction, such as carbon monoxide (CO) and adsorbed water molecules, on the electrode surface. These species can inhibit the reaction and reduce the efficiency of glucose oxidation [12].

To overcome these challenges and improve the electrooxidation of glucose, researchers have explored various strategies. One common approach is to modify the electrode surface by depositing catalysts or nanostructured materials that can enhance the reaction kinetics and facilitate glucose oxidation. For instance, the use of platinum-based nanoparticles, alloy, or bimetallic materials have shown improved catalytic activity and stability toward GOR (glucose oxidation reactions) [14]. Wang et al. reported synthesis of ternary PtPdCu nanowires catalyst, which demonstrated significant efficiency for GOR, achieving 2.6 times the performance of Pt/C catalysts [15]. Pt-Pb alloy electrodes were found to be more selective toward GOR [16]. However, the same found to undergo surface poisoning in the presence of Cl⁻ ions. In other studies, Pt surface was modified using Tl, Bi, Sn, Co, and WO_3 and were reported to exhibit higher catalytic activity [17–19]. But heavy metal toxicity prevented their use for practical applications.

In recent years, emerging technologies and nanomaterial advancements have opened new possibilities for improving the catalytic efficiency. For example, the integration of nanostructured materials, such as Pt nanotubes, [20] nanoflowers, [21, 22] mesoporous Pt films, [23] into the electrode architecture can enhance the electrode's surface area, facilitate charge transfer, and provide ample opportunities to customize surface chemistry through functionalization. This creates a favorable environment for efficient glucose oxidation by increasing the number of available binding sites. Xu et al. reported the synthesis of Pt concave nanocubes to be used as abiotic catalysts in the electrocatalytic oxidation of glucose [24]. Pt nanoflower (Pt NF) catalyst has also been employed as the anode material for abiotic Glucose Fuel Cells under neutral conditions [22]. In another study, Lu et al. reported synthesis of porous Pt nanospheres incorporated with glucose oxidase molecules for synergistic cancer therapy [25].

Electrooxidation of glucose at mesoporous Pt electrodes refers to the electrochemical process of oxidizing glucose
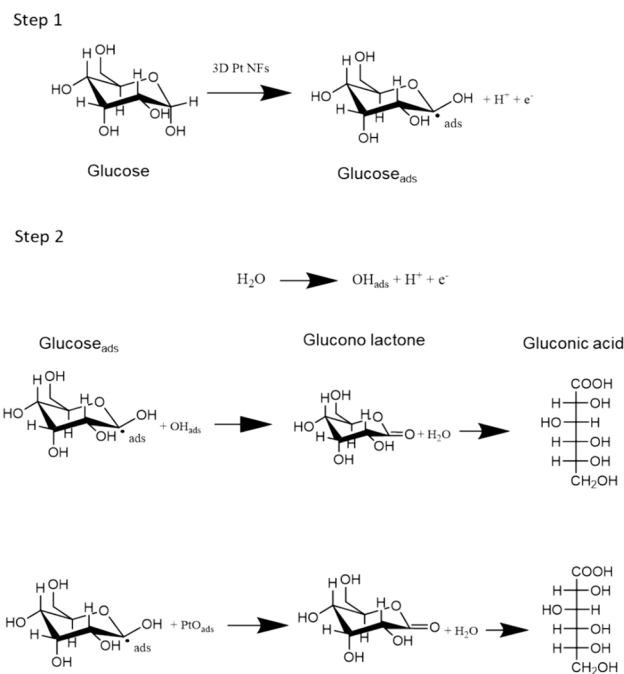
Scheme 1 Mechanism of oxidation at Pt electrode

molecules using mesoporous platinum (Pt) electrodes as the catalyst. The mechanism of electrooxidation of glucose is not fully understood [8, 26]. Mele et al. elucidated the mechanism of glucose oxidation at Pt electrodes, a topic extensively reviewed and discussed in subsequent studies [27]. Step wise mechanism of glucose oxidation is shown in Scheme 1. It has been suggested that the electrooxidation of glucose at Pt electrodes involves several steps. First, glucose molecules in the presence of an electrolyte are adsorbed onto the Pt surface followed by oxidation, typically through a series of redox reactions, resulting in the release of electrons and protons. The electrons are then transferred through the Pt electrode, while the protons migrate through the electrolyte [13, 28].

During electrochemical reactions, species in close proximity to electrode surface are generally detected. Therefore, electrode surface plays a crucial role in their electrochemical performance. Nanoporous Pt electrodes possess large surface area and facilitates mass transport of reactants and products. Their distinctive configuration results in heightened electrocatalytic activity and superior GOR performance when contrasted with traditional Pt electrodes. Park et al. [23] reported enhanced electrochemical oxidation of glucose at mesoporous Pt films. The oxidation process at mesoporous Pt electrodes closely resembles glucose oxidation at conventional flat surface Pt electrodes. However, as compared to conventional electrodes, mesoporous Pt electrodes offered great sensitivity toward glucose electrooxidation even in the

presence of interfering species like L-ascorbic acid and 4-acetamidophenol.

Ongoing research aims to exploit the use of ordered 3D Pt nanomaterials to improve the performance and stability of glucose electrooxidation systems. In this work, we adopted a simple and versatile method as described in detail by Akbar et al. [29] The deposition route adopted in the study is advantageous over many other production techniques reported in literature. For example, Pt ordered 3D materials has been produced using hard templates like mesoporous silica and anodic aluminum oxide, which are themselves created from block copolymers [30–32]. These synthesis methods include lengthy procedures, high temperature, and the use of harsh chemicals for template removal. In contrast, we utilized a straightforward procedure under mild conditions. In our study, the surfactant (Phytantriol) spontaneously self-assembles into a structure with double diamond morphology in the presence of aqueous solvent. Following electrodeposition, ethanol can easily wash away the template, eliminating the use of harsh chemicals.

The Pt nanomaterials produced in this study are free-standing, allowing for the creation of interconnected 3D networks of Pt nanowires without the need for additional conductive support. This interconnection among the Pt nanowires prevents aggregation and restacking, which confers several benefits, including increased accessible surface area, heightened electrocatalytic activity, efficient electron transfer, enhanced sensitivity, selectivity, and structural robustness. These merits position it as a highly promising electrode material across a range of applications, encompassing fuel cells, biosensors, and other electrochemical devices. The integration of such networks holds the potential to advance the creation of more efficient and high-performing electrochemical systems.

2 Results and discussion

Hexachloroplatinic acid (8wt% in water) is used as a platinum precursor solution and phytantriol-based double diamond bicontinuous cubic phase of symmetry *Pn3m* is used as a template. Within the aqueous channels of the cubic phase, platinum is electrodeposited using potential hold at − 0.2 V vs Ag/AgCl reference electrode. After electrodeposition, phytantriol template is removed by dissolving into ethanol. Figure 1 shows 1D small angle X-Ray diffraction patterns from the cubic template and the resultant 3D Pt nanowire frameworks.

ID SAXS pattern for phytantriol template in excess HCPA solution exhibits four Braggs peak with relative position for 1/d in ratios $\sqrt{2}: \sqrt{3}: \sqrt{4}: \sqrt{6}$ which can be indexed as $hkl = 110, 111, 200,$ and 211 reflections of a bicontinuous cubic phase of *Pn3m* symmetry of crystallographic space

group Q_{224}. Lattice parameter values are estimated to be 67.64 ± 0.04 Å. After fabrication and removal of the template, 1D SAXS pattern of Pt nanowire framework shows two Braggs peak with their relative positions for 1/d in ratios $\sqrt{3}: \sqrt{8}$, consistent with single diamond morphology of Fd3m symmetry of crystallographic space group Q_{227}. Lattice parameter values are estimated to be 126.59 ± 16.7 Å, almost a two-fold increase from the value (67.6 Å) of the double diamond structure of the template. The results are in good agreement with our previous findings [29, 33]. Lipid bicontinuous cubic phases exhibit three-dimensional symmetry, a substantial surface area to volume ratio, and an exceptionally organized network of two continuous non-intersecting aqueous channels. These channels of uniform diameter are separated by lipid bilayer. The preservation of bilayer continuity is proposed to involve sealing one of the water channel networks with the bilayer, while the other network remains open to the bulk water [34]. Our observations are consistent with this notion, as SAXS analysis of the template and the resulting replica suggested that only the open-channel network was replicated into cubic frameworks of Pt with diamond symmetry without disrupting the crystalline order.

Further details about the structure and morphology of the fabricated Pt NFs can be seen in the TEM images shown in Fig. 2. The 3D Pt NFs refers to the interconnected arrangement of Pt nanowires, forming a complex and intricate architecture in three dimensions. This network structure exhibits high degree of organization and regularity, resulting in long range order throughout the material as shown in high resolution TEM images. Upon enlarging a section of the TEM image, the intricate nature of 3D Pt NFs becomes more apparent. Figure 2B shows TEM image with superimposed simulation projection drawn to scale with respect to SAXS data. Long range order is clearly visible as a repeating structural feature which may manifest as evenly spaced interconnected nanowires. From TEM data, nanowire diameter is estimated to be 3 nm and interwire distance is calculated to be 9 nm.

Electrocatalytic activity of both conventional and 3D Pt NFs electrodes toward glucose oxidation reaction (GOR) is studied using cyclic voltammetry technique. Roughness factor (Rf) is used to measure the electroactive surface area of the electrode. For conventional Pt electrode, Rf value is estimated to be 2.1. After electrodeposition of 3D Pt NFs, Rf value of the respective electrode was increased to 250, i.e. the Rf value of the 3D Pt NFs electrode is significantly enhanced by 150-fold. The electrochemically active surface (ECSA) of 3D Pt NFs are determined to be 40 m^2 g^{-1}. [29] When compared to graphene-supported Pt nanowires which feature 12–33 m^2 g^{-1}, [35] the Pt utilization in the 3D Pt NFs is significantly higher. Consequently, current densities for glucose oxidation measured by CV have increased,
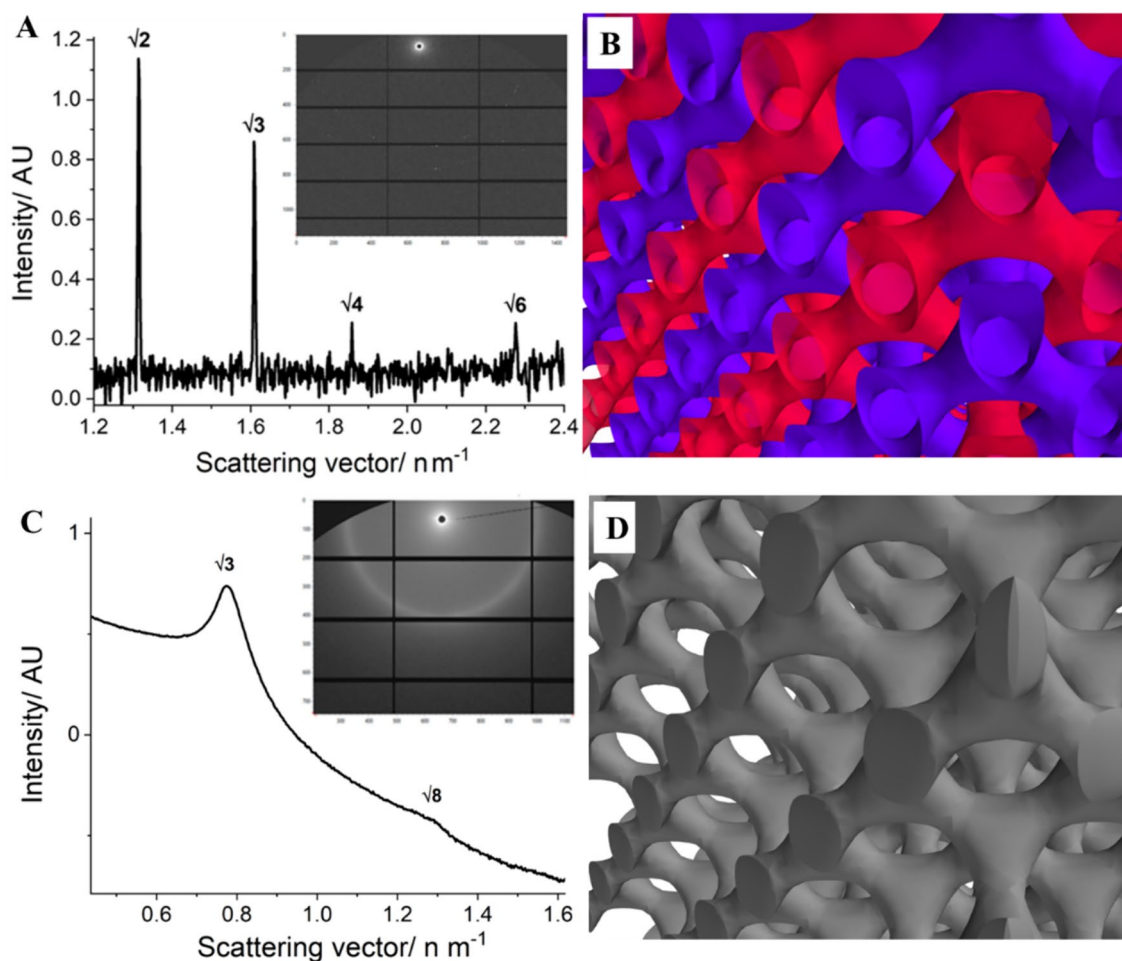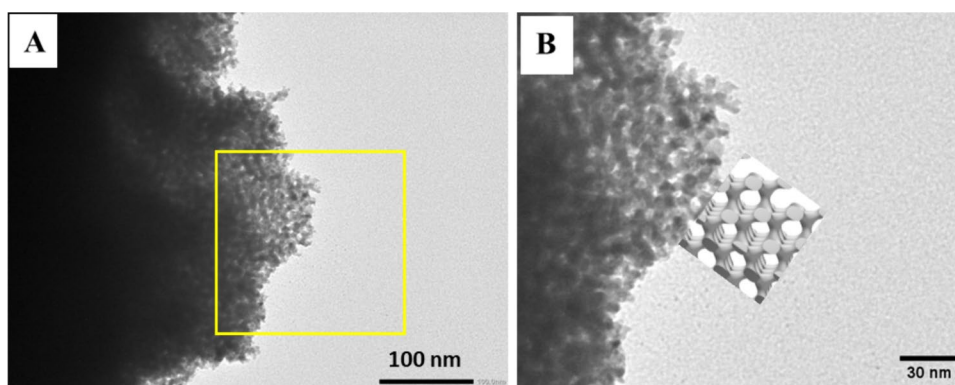
Fig. 1 1D SAXS profiles and 3D cartoon structure of phytantriol cubic template (**A**, **B**) and the fabricated 3D Pt nanowire frameworks (**C**, **D**). Inset (**A**, **C**) shows 2D SAXS profiles

Fig. 2 **A** High resolution TEM images of fabricated 3D Pt nanowire frameworks, **B** Enlarged section from boxed area of (**A**) with superimposed simulation projection drawn to scale with respect to SAXS data

reflecting the quantitative enhancement of the electrode's surface roughness.

Compared to the ECSA of other graphene-supported nanostructured Pt materials,

Typical cyclic voltammograms of conventional Pt electrodes in 0.1 M NaOH solution in the presence and absence of glucose recorded at a scan rate of 50 mV s^{-1} are shown in Fig. 3. In the absence of glucose, Pt oxidation takes place in the region between $+0.45$ and -0.9 V vs Ag/AgCl to form oxide layer at the surface of Pt. During reverse scan, metal oxide reduction peak appears at -0.15 V with a cathodic peak current density of 0.91 mA cm^{-2}.
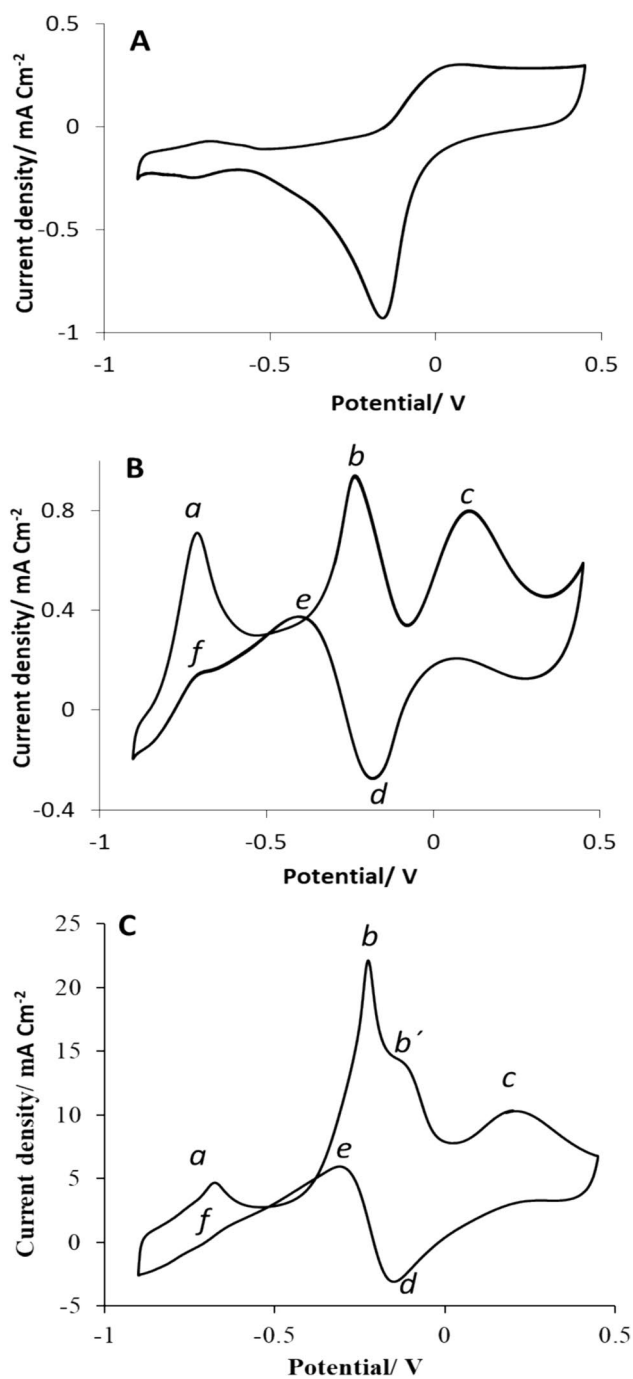
Fig. 3 Cyclic voltammogram of **A** polished electrode in the 0.1 M NaOH at 50 mV s^{-1}, **B** polished platinum electrode (1.96 × 10^{-3} cm^2 area) in 20 mM glucose + 0.1 M NaOH solution, **C** nanostructured Pt electrode in 20 mM glucose + 0.1 M NaOH solution. All CVs are recorded between the limits + 0.45 to − 0.9 V vs Ag/AgCl at room temperature at a scan rate of 50 mV s.$^{-1}$

In the presence of 20 mM glucose, GOR at conventional Pt electrode was detected in three anodic peaks during positive scan at − 0.69 V (peak *a*), − 0.22 V (peak *b*) and 0.22 to 0.13 V (peak *c*) vs Ag/AgCl. Current densities were estimated

to be 0.71, 0.9 and 0.78 mA cm^{-2} for peak *a, b* and *c* respectively. On the −ve scan, glucose is reduced after the reduction of Pt-oxide layer. With a slight potential shift from − 0.16 to − 0.17 V, PtO reduction peak current density is greatly reduced from 1.6 to 0.275 mA cm^{-2}, generating more active sites available for glucose oxidation causing oxidation peaks at − 0.4 (peak e) and − 0.7 (peak f) V with the current density of 0.38 and 0.145 mA cm^{-2}. Electrosorption of hydrogen atoms in the region − 0.5 to − 0.9 V vs Ag/AgCl is hindered in the solution containing glucose. The observations are consistent with the previous findings [12, 36]. the appearance of anodic peak *f* during -ve scan in the same potential range as of peak *a* during + ve going scan represent characteristics of surface absorbed species. Which is further supported by the fact that peak potential of *a* also does not vary with the scan rate as shown in Fig. 5. The peaks b and c represent oxidation of absorbate specie and bulk glucose on Pt electrode surface.

The nature of glucose oxidation products has been a topic of debate for the past two decades. Various studies have reported gluconic acid [37], carbon dioxide [38], and gluconolactone [39] as the primary products resulting from the oxidation of glucose. Among these, gluconic acid has also been detected in the solution [37]. However, there is evidence suggesting that gluconic acid may actually be formed through the hydrolysis of gluconolactone, which has been identified as a significant electrolysis product using field desorption mass spectroscopy [39]. It is plausible that both substances could be generated at relatively low potential levels.

For GOR at 3D Pt NFs electrode, a very sharp anodic peak (*b*) is detected at − 0.22 V with the current density of 23.157 mA cm^{-2}. Anodic peak *c* appears at 0.23 V with the current density of 12.1 mA cm^{-2}. Another small anodic peak (*b′*) appeared at − 0.115 V with the current density of 16.3 mA cm^{-2}. Lower glucose oxidation peak potentials, accompanied by a significant increase in peak current density, indicate the prompt electrooxidation of glucose, which is attributed to the higher electrocatalytic activity of Pt nanowire electrode. Values recorded for peak current densities and peak potentials are shown in Tables 1 and 2.

For electrocatalytic reactions, high surface area is extremely desirable as it allows for more efficient interactions with ions in electrical processes. 3D Pt NFs electrodes exhibits three-dimensional structure, which possess a complex and intricate network of nanoscale features. The three-dimensional arrangement of nanowires results in a substantial exposed surface area which in turn provides more active sites for reactant molecules to encounter the catalyst, thus increasing the rate of glucose adsorption and oxidation. The porous structure also facilitates the diffusion of reactant and products, enabling better mass transport during the electrochemical reaction. Further, at the nanoscale, materials may exhibit different electronic and chemical properties compared to their bulk counterparts.

Table 1 Current density values

Current densities (*j*) mA/cm^2	J_a	J_b	J_c	J_d	J_e	J_f	J_b/J_e
Conventional Pt electrode	0.71	0.9	0.78	0.27	0.38	0.14	2.37
3D Pt NFs	4.73	23.1	12.1	2.46	7.21	1.2	3.21

These altered properties can make the nanomaterials highly reactive and efficient catalysts for electrochemical reactions.

Furthermore, electrocatalytic response of 3D Pt NFs towards GOR in both forward and reverse scans is comparable. On reverse (−ve) scan glucose oxidation peak (d) appears at − 0.3 V with the current density of 7.21 mA cm^{-2}. The ratio between forward and backward oxidation peak current densities (*jb/je*), is often used to describe the tolerance of catalysts against the incompletely oxidized species which are accumulated on their surfaces [36]. A large ratio means good tolerance of the anode against the poisoning species, i.e., more effective removal of the poisoning species on the electrode surface during + ve sweep. The peak current density ratios (*jb/je*) for GOR at conventional Pt electrode is estimated to be 2.37 which was increased to 3.2 when GOR is carried out at 3D Pt NFs electrode, which is higher than the value 0.9 (Pt/p-1,8-DAN/GC) [36] reported previously. This indicates much higher electrocatalytic efficiency of the nanostructured Pt electrode for glucose oxidation reactions. Mello et al. reported a reduction of current density of main oxidation peak during repetitive cycling which was attributed to the adsorption of poisoning species at the surface of electrodes [40]. For 3D Pt NFs, reduction in the peak current densities is negligible after repetitive cycling, as shown in supporting information (Figure S1). Form comparison of 1st and 50th CV, peak current density for peak b is only reduced from 23 to 22.4 mA cm^{-2}. These outcomes clearly indicate the impact of nanoarchitecture of 3D Pt NFs on the kinetics of glucose electrooxidation. Transport characteristics dependence of glucose oxidation at both polished and fabricated 3D Pt NFs electrodes, is investigated by recording cyclic voltammograms at different scan rates. Using a range of scan rates from 50 to 250 mV s^{-1}, it is determined how transport parameters affect the oxidation of glucose at Pt catalysts. A multi scan CV is shown in Fig. 4.

At both electrodes, linear relationship of peak current density with respect to square root of scan rate shows diffusion control contributes to the intricate electron transfer oxidation process in the direction of the positive going sweep, as shown in Fig. 4. Values are given in supporting information (Tables 1, 2).

3D Pt NFs is tested for electrooxidation of glucose within the physiological level (3 − 8 mM). CVs for conventional Pt electrode and nanostructured Pt electrode in the presence of 4 mM glucose in 0.1 M NaOH solution are shown in Fig. 5.

At conventional Pt electrode, cyclic voltammogram shows prominent Pt oxidation and reduction regions. A small glucose oxidation peak (*b*) is observed at ~ − 0.2 V with the current density of 0.34 mA cm^{-2}. However, at 3D Pt NFs electrode, Pt oxidation and reduction signals are suppressed due to higher catalytic response toward GOR. A prominent glucose oxidation peak appeared at − 0.24 v with the current density of 15.4 mA cm^{-2}. Enhanced GOR response at nanostructured Pt electrode implies that electrodes with a three-dimensional nanostructured surface are capable of detecting glucose even when it is present in very small or trace amounts.

3 Conclusion

In summary, the research demonstrates that 3D Pt NFs electrodes outperform conventional Pt electrodes in electrocatalytic glucose oxidation reactions. This superior performance is attributed to the large surface area and unique structure of the 3D Pt NFs, which facilitate a higher density of glucose adsorption sites and efficient glucose utilization. This, in turn, promotes efficient electron transfer and reduces the need for high Pt loading, resulting in improved glucose oxidation efficiency, faster reaction kinetics, and enhanced stability. The application of mesoporous Pt electrodes in glucose oxidation holds significant potential in improving fuel cell performance, biosensing, and other electrochemical applications.

4 Experimental section

4.1 Materials

Phytantriol acquired from TCI Europe is utilized as the surfactant phase, and hexachloroplatinic acid (HCPA) solution (8 wt% in water), purchased from Sigma Aldrich, is employed as a platinum precursor. From concentrated acid of Merck p.a. grade, aqueous sulfuric acid (H$_2$SO$_4$) solution (0.5 M) was prepared. Ethanol and glucose are purchased from Fischer Scientific. Highly purified water was obtained

Table 2 Peak potential values

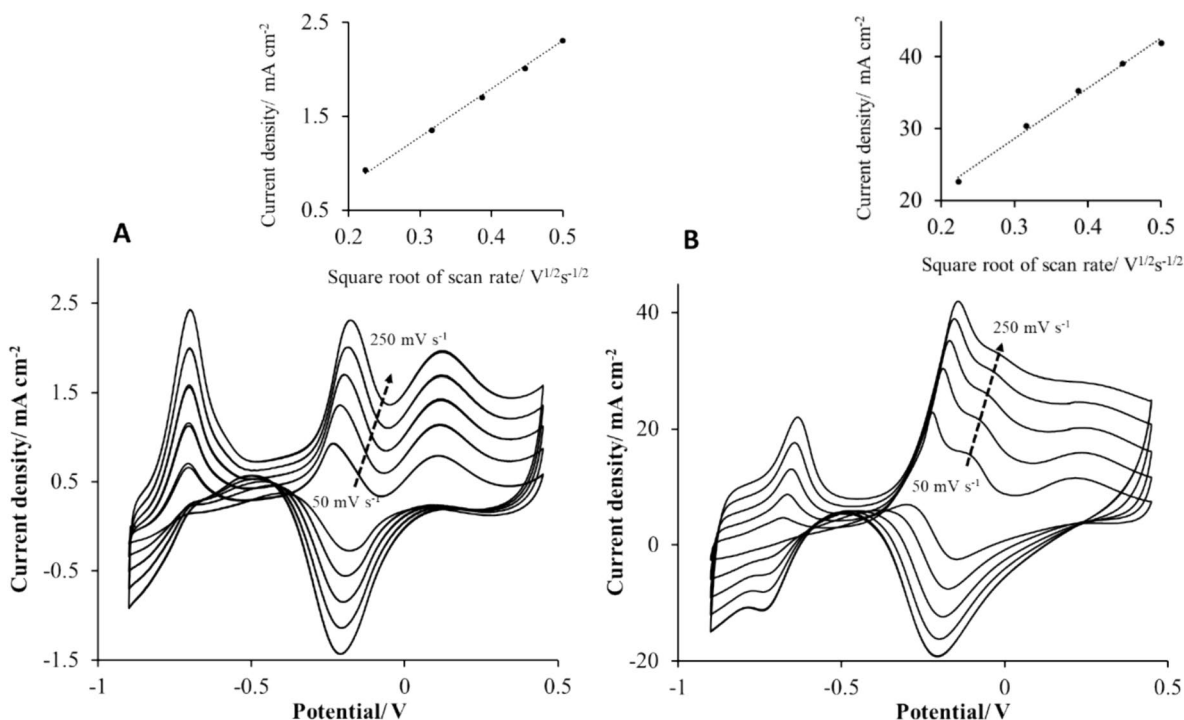| Peak potential (E)/ V	E_a	E_b	E_c	E_d	E_e	E_f
Conventional Pt electrode	− 0.70	− 0.22	0.13	− 0.17	− 0.40	− 0.70
3D Pt NFs	− 0.68	− 0.22	0.23	− 0.15	− 0.30	− 0.65

Fig. 4 A multi scan CV for conventional Pt electrode (**A**) and 3D Pt NFs in 20 mM glucose in 0.1 M NaOH solution recorded between the limits + 0.45 to − 0.9 V vs Ag/AgCl at room temperature. Inset shows relationship of peak current density with respect to scan rate
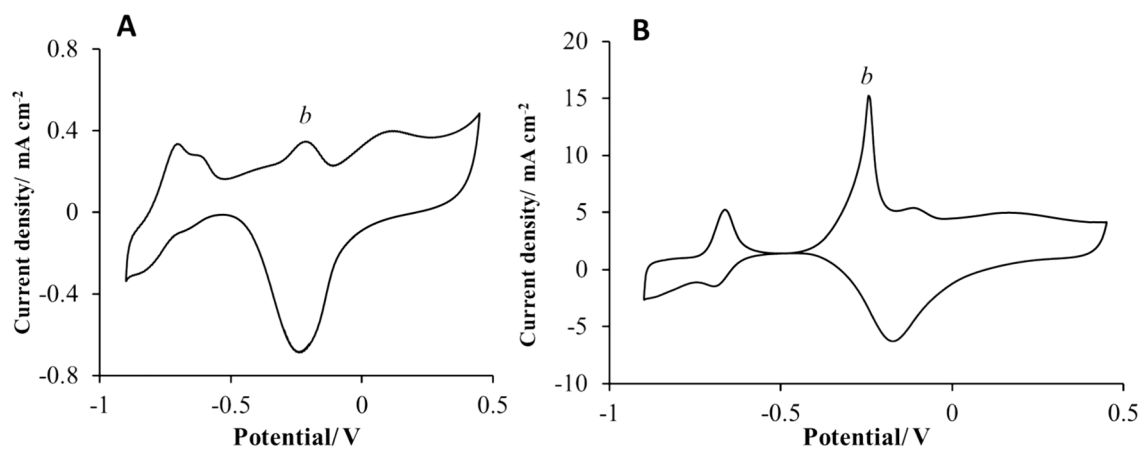

Fig. 5 Cyclic voltammograms for **A** conventional Pt electrode and **B** nanostructured Pt electrode in the presence of 4 mM glucose in 0.1 M NaOH solution

by passing deionized, distilled water through Puris Expe-CB Ultra Purification system.

4.2 Electrochemical investigations

Electrochemical studies were carried out using Gamry interface 1000 in a standard 3-electrode cell composed of a platinum gauze counter electrode, a Ag/AgCl reference electrode, and a 0.5 mm Pt disc electrode. At room temperature, electrochemical studies are performed in a Pyrex cell of volume 25 ml. Sandpaper and alumina powder in three different grades (25, 1.0, and 0.3 μm) are used to polish platinum disc electrodes sealed in a glass tubing. After polishing, the electrodes are repeatedly scanned by cyclic voltammetry in 0.5 M aqueous H_2SO_4 solution using different scan rates in the range of possible limits 1.23 and − 0.2 V vs Ag/AgCl until sharp hydrogen adsorption/desorption peaks are visible.

Single diamond Pt nanowire framework are synthesized following the procedure described in detail by Akbar et al. [29] Platinum disc electrodes with 1.96×10^{-3} cm^2 area are used for electrochemical investigations. For SAXS and TEM analysis, Gold archival DVD of area 0.5–1 cm^2 from Delkin Devices are used as working electrodes.

4.3 Samples of phytantriol under conditions of excessive hydration

For SAXS analysis of the template, on the inside of open-ended, thin-walled glass capillary tubes, phytantriol is thinly coated from a 1:1 w/w phytantriol ethanolic solution, dried with compressed air for about 15 min, and then stored at room temperature for at least an hour. For immediate use, the duration of drying with compressed air was increased to ~30 min. A small layer of phytantriol was left when the ethanol evaporated at this period. HCPA solution (8 wt% in water) or water is then added to the capillary and sealed for SAXS analysis.

4.4 Preparation of working electrode

By soaking into an ethanolic mixture of phytantriol (w/w ratio of 1:2), a thin layer of phytantriol is applied to a variety of bare working electrodes, then drying for at least two hours at room temperature. The ethanol evaporated over this period, leaving a surfactant layer (approx. 16 micron thick) at the surface of the electrode. Surfactant-coated electrodes were soaked in HCPA solution for at least 10 min prior to electrodeposition. For stochiometric deposition, potential was stepped from $+0.6$ to -0.2 V vs Ag/AgCl in excess HCPA solution (8 wt%). After deposition, electrodes are washed using ethanol and water to remove the surfactant template.

4.5 Physical analysis

Small Angle X-ray Scattering (SAXS) experiments were performed at Diamond Light Source using beamline 122 in transmission mode with detector distance of 4752 mm and energy 12.4 keV. TEM analysis was carried out using model JSM-2100PLUS.

Author contributions All authors contributed to the study conception and design. Material preparation, data collection and analysis were performed by Tamseel Zaman and Joshua White. Samina Akbar and Iris Nandhakumar supervised the research and provided the lab facilities.

The first draft of the manuscript was written by Tamseel Zaman. All authors read and approved the final manuscript.

Declarations

Conflict of interest The authors declare no conflict of interest.

References

1. Katz E, MacVittie K (2013) Energy Environ Sci 6:2791–2803
2. Basu D, Basu S (2010) Electrochim Acta 55:5775–5779
3. N. Neha, T. Rafaïdeen, T. Faverge, F. Maillard, M. Chatenet, C. Coutanceau (2022) Electrocatalysis 14: 121–130
4. Cosnier S, Gross AJ, Le Goff A, Holzinger M (2016) J Power Sources 325:252–263
5. Cosnier S, Le Goff A, Holzinger M (2014) Electrochem Commun 38:19–23
6. Heller A, Feldman B (2008) Chem Rev 108:2482–2505
7. McCormick W, McCrudden D (2020) J Electroanal Chem 860:113912
8. Bolzan A, Iwasita T, Vielstich W (1987) J Electrochem Soc 134:3052
9. Ryu J, Kim K, Kim H-S, Hahn HT, Lashmore D (2010) Biosens Bioelectron 26:602–607
10. Skou E (1977) Electrochim Acta 22:313–318
11. Bae I, Yeager E, Xing X, Liu C (1991) J Electroanal Chem Interfacial Electrochem 309:131–145
12. Lei H-W, Wu B, Cha C-S, Kita H (1995) J Electroanal Chem 382:103–110
13. Mello GA, Briega-Martos V, Feliu JM (2022) J Electroanal Chem 924:116850
14. Basu D, Basu S (2011) Int J Hydrogen Energy 36:14923–14929
15. Wang K, He S, Zhang B, Cao Z, Zhou T, He J, Chu G (2023) Molecules 28:5834
16. Cui H-F, Ye J-S, Liu X, Zhang W-D, Sheu F-S (2006) Nanotechnology 17:2334
17. Wittstock G, Strübing A, Szargan R, Werner G (1998) J Electroanal Chem 444:61–73
18. Karski S, Paryjczak T, Witonñska I (2003) Kinet Catal 44:618–622
19. Zhang X, Chan K-Y, You J-K, Lin Z-G, Tseung AC (1997) J Electroanal Chem 430:147–153
20. Yang H, Shi Q, Song Y, Li X, Zhu C, Du D, Lin Y (2017) J Electrochem Soc 164:B230
21. Guo M, Hong H, Tang X, Fang H, Xu X (2012) Electrochim Acta 63:1–8

22. Xu X, Dong X, Li D, Qi M, Huang H (2023) ACS Appl Mater Interfaces 15:17969–17977
23. Park S, Chung TD, Kim HC (2003) Anal Chem 75:3046–3049
24. Xu X, Ma Z, Li D, Su Z, Dong X, Huang H, Qi M (2022) ACS Appl Nano Mater 5:4983–4990
25. Lu Z, Gao J, Fang C, Zhou Y, Li X, Han G (2020) Adv Science 7:2001223
26. Beden B, Largeaud F, Kokoh K, Lamy C (1996) Electrochim Acta 41:701–709
27. De Mele M, Videla HA, Arvia AJ (1982) J Electrochem Soc 129:2207
28. Mello GA, Cheuquepán W, Briega-Martos V (2020) J M J E A Feliu 354:136765
29. Akbar S, Elliott JM, Rittman M, Squires AM (2013) Adv Mater 8:1160–1164
30. Chen P-K, Lai N-C, Ho C-H, Hu Y-W, Lee J-F, Yang C-M (2013) Chem Mater 25:4269–4277
31. Wang Z, Mai Y, Yang Y, Shen L, Yan C (2021) ACS Appl Mater Interfaces 13:38138–38146
32. Tao W, Pan D, Gong Z, Peng X (2018) Anal Chim Acta 1035:44–50
33. Akbar S, Elliott JM, Squires AM, Anwar A (2020) J Nanopart Res 22:1–9
34. Larsson K (2000) Curr Opin Colloid Interface Sci 5:64–69
35. Qazzazie D, Yurchenko O, Urban S, Kieninger J, Urban G (2017) Nanoscale 9:6436–6447
36. Hassan KM, Khalifa Z, Elhaddad GM, Azzem MA (2020) Electrochim Acta 355:136781
37. Rao MB, Drake RF (1969) J Electrochem Soc 116:334
38. Marinčić L, Soeldner JS, Colton CK, Giner J, Morris S (1979) J Electrochem Soc 126:43
39. Ernst S, Heitbaum J, Hamann C (1980) Ber Bunsenges Phys Chem 84:50–55
40. Mello GA, Cheuquepán W, Feliu JM (2020) J Electroanal Chem 878:114549

Publisher's Note Springer Nature remains neutral with regard to jurisdictional claims in published maps and institutional affiliations.